

GASPACHO: Gaussian Splatting for Controllable Humans and Objects

Aymen Mir^{1,2*} Arthur Moreau¹ Helisa Dhama^{1§} Zhensong Zhang¹ Eduardo Pérez-Pellitero¹

¹Huawei Noah’s Ark Lab, London

²University of Tübingen, Germany



Figure 1. **Left.** Using sparse or dense (4 to 48) multi-view RGB images of human-object interactions, our method jointly reconstructs animatable models of the human and the object. **Right** The reconstructed model can be driven by control signals to synthesize photo-real *novel pairs* of human-object interactions with *free camera viewpoint control*.

Abstract

We present GASPACHO: a method for generating photo-realistic controllable renderings of human-object interactions. Given a set of multi-view RGB images of human-object interactions, our method reconstructs animatable templates of the human and object as separate sets of Gaussians simultaneously. Different from existing work, which focuses on human reconstruction and ignores objects as background, our method explicitly reconstructs both humans and objects, thereby allowing for controllable renderings of novel human object interactions in different poses from novel-camera viewpoints. During reconstruction, we constrain the Gaussians that generate rendered images to be a linear function of a set of canonical Gaussians. By simply changing the parameters of the linear deformation functions after training, our method can generate renderings of novel human-object interaction in novel poses from novel camera viewpoints. We learn the 3D Gaussian properties of

the canonical Gaussians on the underlying 2D manifold of the canonical human and object templates. This in turns requires a canonical object template with a fixed UV unwrapping. To define such an object template, we use a feature based representation to track the object across the multi-view sequence. We further propose an occlusion aware photometric loss that allows for reconstructions under significant occlusions. Several experiments on two human-object datasets - BEHAVE and DNA-Rendering - demonstrate that our method allows for high-quality reconstruction of human and object templates under significant occlusion and the synthesis of controllable renderings of novel human-object interactions in novel human poses from novel camera views.

1. Introduction

Photorealistic Novel View Synthesis of animatable human avatars is essential for several applications ranging from telepresence, AR/VR, special effects to e-commerce. The recent emergence of Gaussian Splatting as a 3D representation [37] has enabled a new wave of efficient methods that reconstruct high-quality animatable human avatars

*Work done as intern at Huawei. §Work done while at Huawei

[38, 46, 55, 57, 62, 72], which can be driven by controllable human pose signals to generate photorealistic images of humans in novel poses. However, these methods assume that the humans reconstructed are *recorded in isolation*, without any occlusions, and when they are animated, their actions are generated in *isolation* often in *empty space*.

In the real world, however, human motion in complete isolation is rare. Our environment constrains our motions and provides affordances. While there exists a body of work on human-object interaction [20, 22, 23, 87, 89], it focuses only on modeling human behaviour in environments and *neglects human appearance*. A few recent papers study the photorealistic reconstruction of human-object interaction, but assume the objects to be static [38, 83], focus only on human-object reconstruction, are unable to synthesize novel human-object interaction [32, 68] or assume the object to be a small extension of one human hand [47, 84].

In this work, we *depart from all prior work* by posing the following two questions: 1) how does one reconstruct separate photorealistic animatable human and object models robustly from multi-view (both sparse and dense) RGB sequences under *significant occlusion*? 2) how does one go beyond photorealistic image synthesis of novel human actions in isolation to synthesize *novel human-object interactions with free camera viewpoint control*? (see Fig. 1)

Addressing these questions should provide a step towards handling the naturally occurring occlusions in real-world recordings of humans, while opening up applications that require photo-real synthesis of human-object interactions and not just the synthesis of humans in isolation.

These questions pose challenges yet unaddressed by existing work. First, while prior work [38, 46, 54, 57] demonstrates the efficacy of using a set of canonical Gaussians to model animatable humans, it remains an open question, in the context of neural fields, how one should model *not just humans* but their interactions with dynamic objects. Second, existing work usually learns high-fidelity animatable human Gaussian models [46, 57] by parameterizing Gaussians as 2D maps. This remains possible only because some mesh based models such as SMPL [49] or GHUM [80] provide a unified representation for the human body which can be used for creating a 2D unwrapping of the human surface. There is no such unified representation for objects. Third, when humans are captured interacting with objects, the inevitable occlusions make it impossible to know the exact color of the occluded human or object for some pixels.

To address these challenges we present several novel insights. First, we model humans and objects separately using two disjoint sets of Gaussians - one for the human and one for the object. To ensure that the human and object models are animatable, we constrain the 3D Gaussians used to generate rendered images to be linear functions [5, 42] of sets of Canonical Gaussians restricted to fixed templates.

By changing the parameters of the linear deformation functions, our method can generate photorealistic renderings of *novel* human-object interaction in novel poses from novel camera viewpoints at test-time. Inspired by prior work [26], to ensure high-fidelity we learn the 3D Gaussian properties on the underlying 2D manifold of the canonical human and object template surface. This in turns requires a canonical object template with a fixed UV unwrapping. To define such a coarse object template and create a fixed UV unwrapping for the object, we use a feature-based 3DGS reconstruction algorithm. We further track this template through multi-view RGB sequence by inverting Gaussian Splatting rasterization to find 6D object parameters that map already constructed Gaussians to RGB images. We also introduce a novel occlusion guided photometric loss that allows for reconstructions of objects and humans separately despite significant occlusions.

To evaluate our method on high-quality dense multi-view images we use the DNA-Rendering [11] dataset. To demonstrate the efficacy of our method on challenging interactions with large objects such as sitting on chairs, which are not present in DNA-Rendering, we also use the BEHAVE [8] dataset. Experiments on BEHAVE also serve to demonstrate the utility of our method for data collected with sparse (only four cameras) low-cost commodity sensors which are mobile and easier to setup for data-capture.

To summarize, our contributions are: 1) We present a novel method to jointly reconstruct humans and objects under occlusion, which can then be animated to synthesize novel human-object interactions from new camera viewpoints. 2) We propose to use a feature based representation to construct a coarse object template that allows for parameterizing object Gaussian properties as 2D maps and for learning high frequency object details. 3) We propose to track objects in a multi-view setting by inverting Gaussian Splatting reconstruction to find 6D object pose parameters that map already constructed Gaussians to RGB images. 4) We introduce an occlusion aware photometric loss to allow for human-object reconstruction under occlusion.

2. Related Work

2.1. Neural Rendering

Since the publication of NeRF [53], there has been an explosion of interest in Neural Rendering [79]. Despite appealing image quality, NeRF is limited by its computational complexity. Though there have been several follow-up improvements [6, 7, 56, 70], the high computational cost of NeRF remains. 3DGS introduced by Kerbl et al. [37] addresses this limitation by representing scenes with an explicit set of primitives shaped as 3D Gaussians, extending previous work using spheres [39]. 3DGS rasterizes Gaussian primitives into images using a splatting algorithm [74].

3DGS originally designed for static scenes has been extended to dynamic scenes [40, 44, 50, 66, 75], slam-based reconstruction, [36], mesh reconstruction [17, 28] and NVS from sparse cameras [52].

2.2. Human Reconstruction and Neural Rendering

Mesh-based templates [49, 60] have been used to recover 3D human shape and pose from images and video [9, 34]. However, the mesh-based representation does not often allow for photorealistic renderings. In [2, 3] Alldieck *et al.* recover a re-posable human avatar from monocular RGB. However their use of a mesh template does not allow for photorealistic renderings. Implicit functions [51, 59] have also been utilized to reconstruct detailed 3D clothed humans [4, 10, 13, 25, 29, 64]. However, they are also unable to generate photorealistic renderings and are often not re-posable. Several works [18, 21, 31, 43, 48, 61, 73, 81, 89] build a controllable NeRF that produces photorealistic images of humans from input videos. However they inherit the speed and quality restrictions of the original NeRF formulation. Furthermore, unlike us, they do not model human-object interactions. With the advent of 3DGS, several recent papers use a 3DGS formulation [1, 14, 27, 33, 38, 41, 45, 46, 54, 55, 58, 62, 63, 82, 88, 90] to build controllable human or face avatars. Unlike our method, they do not model human-object interactions or reconstruct humans under occlusion. Prior works have also extended the 3DGS formulation to model humans along with their environment, [83, 84], but unlike us, they either assume that the 3D scene remains static or that its constituent parts are an extension of the human hand.

2.3. Human Object Interaction

Human Object Interaction is another recurrent topic of study in computer vision and graphics. Early works [16, 19, 71] model affordances and human-object interactions using monocular RGB. The collection of several recent human-object interaction datasets [8, 12, 20, 22, 23, 30, 65, 69, 87] has allowed the computer vision community to make significant progress in joint 3D reconstruction of human-object interactions [76–78, 85]. These datasets have also led to the development of methods that synthesize object conditioned controllable human motion [15, 24, 67, 87]. All these methods represent humans and objects as 3D meshes and as such inherit all the limitations of mesh-based representations including their inability to generate photorealistic images, while our method allows for photorealistic renderings of humans and objects.

3. Background: Gaussian Splatting

3DGS [37] uses a set of 3D Gaussians to represent 3D scenes. Each Gaussian is parametrized by its position mean

μ , covariance matrix Σ , opacity α and color c . The probability density function associated with each Gaussian is:

$$f(\mathbf{x}|\mu, \Sigma) = \exp\left(-\frac{1}{2}(\mathbf{x} - \mu)^\top \Sigma^{-1}(\mathbf{x} - \mu)\right). \quad (1)$$

For rendering an image, the 3D Gaussians are splatted onto 2D planes, resulting in 2D Gaussians. The pixel color \mathbf{C} is computed by blending N ordered 2D Gaussians corresponding to this pixel: $\mathbf{C} = \sum_{i=1}^N \alpha_i \prod_{j=1}^{i-1} (1 - \alpha_j) \mathbf{c}_i$ where \mathbf{c}_i is the color of every 2D Gaussian, and α_i is the blending weight obtained from the learnt opacity and 2D Gaussian distribution. For more details see [91].

4. Method

Our method receives a set of multi-view RGB images of humans interacting with objects, captured from N cameras at T temporal frames, $\{\mathbf{I}_t^c\}_{t=1, c=1}^{t=T, c=N}$, along with estimates of camera parameters $\{\gamma_t^c\}_{t=1, c=1}^{t=T, c=N}$ and human pose $\{\theta_t\}_{t=1}^T$. We aim to learn a deformable function $f(\theta, \phi; \gamma)$ that maps new human θ and object poses ϕ to RGB images rendered from novel viewpoints γ . Intuitively, we are interested in a function that allows us to map human and object poses to 3D Gaussians, which can be used to render novel human-object interactions with free camera viewpoint control.

We first use a feature-based representation to construct coarse object templates (Sec. 4.1) and track the template across the temporal frames (Sec. 4.2) to obtain estimates of object pose parameters. Using the estimated object template and the SMPL mesh we define 2D canonical human and object Gaussian maps to learn Gaussian properties (Sec. 4.3) of two sets of Gaussians \mathcal{G}_O and \mathcal{G}_H anchored to the canonical object and SMPL templates respectively. These are deformed using the provided human and estimated object pose parameters to posed space (Sec. 4.4) and learnt using an occlusion guided photometric loss (Sec. 4.5).

4.1. Feature-Based Coarse Object Template

To model object motion, we first need to obtain a suitable reference, i.e. an object template, which will serve as a canonicalized 3D representation. In presence of significant occlusion, we found that obtaining such template via the original 3DGS [37] does not converge (see Tab. 3). Instead, we learn the 3D template model in feature space, so that we can incorporate priors during learning. Specifically, we learn $H \times W$, l -dimensional planes $\mathbf{F}_O \in \mathbb{R}^{3 \times H \times W \times l}$. Next, each Gaussian location \mathbf{x}_k is projected onto each of the three feature planes to obtain feature vectors via bilinear interpolation. These features are then concatenated along the feature dimension. We denote this operation as $\mathbf{f}_k = \pi(\mathbf{x}_k; \mathbf{F}) \in \mathbb{R}^{3l}$. Using multiple small MLPs we map these feature vectors onto Gaussian parameters.

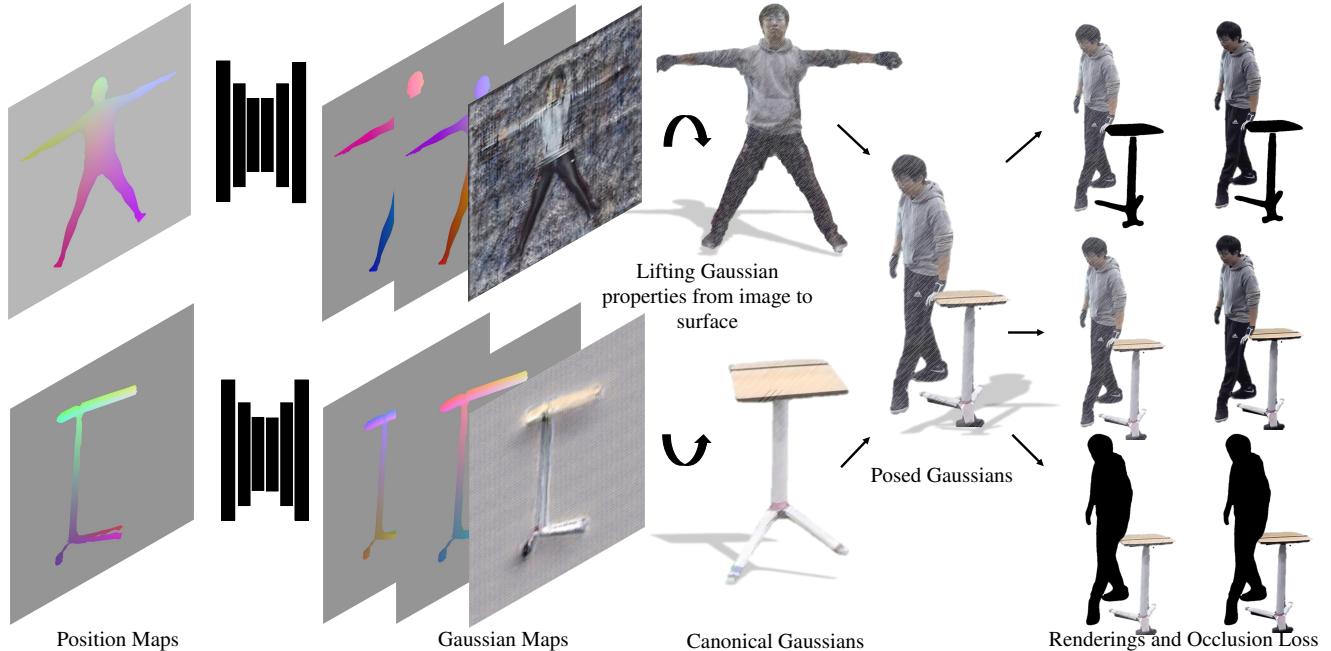


Figure 2. **Method Overview:** Using position maps as input, we learn Gaussian parameters for Gaussians anchored to canonical human and object templates. Gaussian properties - orientation, scale, opacity, color - are learnt as 2D maps structured according to a UV unwrapping of canonical human and object templates. Each pixel thus corresponds to a Gaussian in the canonical template. Once mapped to canonical Gaussians, these Gaussians are posed using LBS for the human and a rigid transform for the object. We render the posed object and human Gaussians separately and compare against the segmented portions of the ground truth image. We further guide the reconstruction using known occlusion information. In the figure above, the black regions of the rendered images are masked out thereby allowing our method to deal with occlusions.

First, using one temporal frame t^* with minimal occlusion, we optimize the features, network weights and Gaussian positions to find the 3DGS parameters that best explain the segmented object pixels in the RGB images:

$$\arg \min_{\mathcal{G}_O^*} \sum_{c=1}^N \|\mathcal{R}(\mathcal{G}_O^*; \gamma_c) - \mathbf{O}_{t^*}^c \cdot \mathbf{I}_{t^*}^c\|_2. \quad (2)$$

Here we use $\mathcal{R}(\cdot; \gamma)$ to denote a Gaussian rasterizer with camera parameters γ and \mathbf{O}_t^c as the object mask. This step provides a coarse canonical object Gaussian template \mathcal{G}_O^* .

4.2. Object Tracking

Once we have learnt a set of 3D Gaussians describing one frame \mathcal{G}_O^* , we want to optimize the transformations that map this canonical object to the renderings in subsequent timesteps t . Thus, we apply an optimizable rigid 6D pose transform ϕ to the object template \mathcal{G}_O^* , and minimize the per-pixel error between renderings and ground-truth images

$$\arg \min_{\phi_t} \sum_{c=1}^N \|\mathcal{R}(\mathcal{T}(\mathcal{G}_O^*; \phi_t); \gamma_c) - \mathbf{O}_t^c \cdot \mathbf{I}_t^c\|_2. \quad (3)$$

Here we define $\mathcal{T}(\mathcal{G}_O; \phi)$ to be a rigid transformation on the position and orientation of canonical object Gaussians. Specifically, given a canonical 3D Gaussian, we transform its position \mathbf{p}_c and covariance Σ_c attributes:

$$\mathbf{p}_p = \mathbf{R}(\phi)\mathbf{p}_c + \mathbf{t}(\phi), \quad \Sigma_p = \mathbf{R}(\phi)\Sigma_c\mathbf{R}(\phi)^\top, \quad (4)$$

where $\mathbf{R}(\phi)$ and $\mathbf{t}(\phi)$ are the rotation and translation components of the 6D object pose ϕ . For tracking convergence we find it essential to initialize the 6D pose parameters at timestep t with those from timestep $t - 1$.

4.3. Gaussian Maps

Using the coarse object template, object pose parameters and the provided SMPL pose parameters, we now aim to learn a mapping from human and object pose parameters to photorealistic RGB images. To this end, we learn properties (scale, opacity, color, orientation) of the two sets of canonical Gaussians \mathcal{G}_O and \mathcal{G}_H in image space which allows for incorporating *powerful inductive biases of 2D CNNs* inspired by prior work [26, 46, 58]. These canonical Gaussians are then posed (Sec. 4.4) to obtain final renderings. To parameterize 3D surface of the human and object as 2D maps, we define UV maps of canonical human and object templates. For the human we do so by projecting the SMPL body model in canonical pose from two front and back views (similar to Fig. 3).

For the object, we project the coarse object - \mathcal{G}_O^* template obtained in Sec. 4.1, from front and back views to compute which Gaussian contributes the highest alpha value during rendering for each pixel (Fig. 3). This creates a one-to-one mapping from rendered pixels to the 3D object template and fully parametrizes the 3D template in image space.

To learn Gaussian properties we employ a StyleGAN-based CNN [35]. To provide pose and shape information

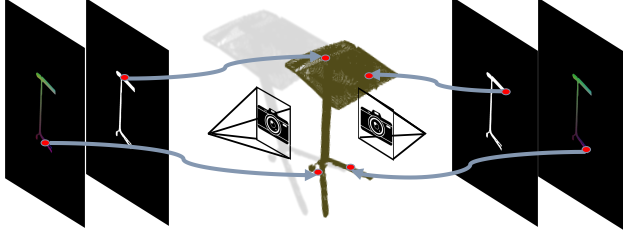


Figure 3. Object UV and Position Maps. By using a perspective projection from the front and back of the canonical coarse object Gaussians, we create a UV map for the object template. The arrows indicate correspondence between pixels and the 3D surface. The rendered images are the Position Maps and contain the 3D gaussian location corresponding to each pixel in the UV map.

to such a 2D CNN, we first create pose-dependent position maps for the human by using LBS to deform the canonical SMPL mesh vertices without any global orientation or translation. Each deformed vertex is stored in the corresponding location of the UV map to define a posed position map (Similar to Fig. 3). For the object we define a fixed pose-independent position map by directly storing the location of the Gaussian in the template (Fig. 3) corresponding to each pixel. We assume that there are no pose-dependent deformations in the object and that the object is fully rigid and use this pose-independent position map in every timestep. Note that in practice, at every timestep t , \mathcal{G}_H changes due to pose-dependent effects while \mathcal{G}_O remains the same.

In the final Gaussian maps predicted by the CNN, each pixel corresponds to a property of the 3D canonical human or object Gaussians (Fig. 2) - covariance matrix, position, opacity etc. By using the one-to-one mapping between the image pixels and the 3D template points, we lift properties from the 2D Gaussian maps onto the 3D Gaussians anchored to the canonical templates (see Fig. 2). In practice we do not predict the positions of the Gaussians directly but merely an offset from the canonical templates. For human Gaussians, in addition to the standard Gaussian properties, we also predict a skinning-weights map, which associates with each Gaussian k a vector of learnt skinning weights \mathbf{w}_k^H

4.4. Deformation

The two sets of Canonical Gaussians are deformed to represent human and object Gaussians in posed space to generate final renderings. For deforming the human Gaussians we use the standard Linear Blend Skinning algorithm with the learnt skinning weights \mathbf{w}^H . For every human Gaussian k , we use the learnt skinning weights to produce a convex combination of the J rotation matrices associated with the J SMPL skeleton joints. $\mathbf{R}_k^H(\boldsymbol{\theta}) = \sum_{j=1}^J \mathbf{w}_{kj}^H \mathbf{R}_j^{SMPL}(\boldsymbol{\theta})$ where the function $\mathbf{R}_j^{SMPL}(\boldsymbol{\theta})$ maps a SMPL pose vector expressed in axis-angles to the corresponding rotation ma-

trix representation of its j^{th} joint. Using the SMPL pose, the position \mathbf{p}_k and covariance Σ_k of the canonical human Gaussian is transformed as

$$\mathbf{p}'_k = \mathbf{R}_k^H(\boldsymbol{\theta})\mathbf{p}_k + \mathbf{t}(\boldsymbol{\theta}), \quad \Sigma'_k = \mathbf{R}_k^H(\boldsymbol{\theta})\Sigma_k\mathbf{R}_k^H(\boldsymbol{\theta})^\top. \quad (5)$$

We denote this transformation of human Gaussians from canonical to posed space as $\mathcal{T}(\mathcal{G}_H; \boldsymbol{\theta})$.

Similarly, every object Gaussian is rigidly transformed using the object pose parameters via the object deformation $\mathcal{T}(\mathcal{G}_O; \phi)$ (Sec. 4.2) to posed space. The deformations only affect the position and orientation of the two canonical Gaussians \mathcal{G}_H and \mathcal{G}_O . The other parameters – scale, color and opacities – remain unchanged.

4.5. Composition and Occlusion Guided Loss

In addition to the GT images from camera c at timestep t \mathbf{I}_t^c , we assume that we have the human mask \mathbf{H}_t^c , and the object-mask \mathbf{O}_t^c as well. Once we obtain the two deformed sets of Gaussians $\mathcal{G}_O^t = \mathcal{T}(\mathcal{G}_O; \phi_t)$, $\mathcal{G}_H^t = \mathcal{T}(\mathcal{G}_H; \boldsymbol{\theta}_t)$, we generate two individually rendered images $\mathbf{I}_{H_t^c}^c = \mathcal{R}(\mathcal{G}_H^t; \gamma_c)$, $\mathbf{I}_{O_t^c}^c = \mathcal{R}(\mathcal{G}_O^t; \gamma_c)$ and a jointly rendered image $\mathbf{I}_{A_t^c}^c = \mathcal{R}(\mathcal{G}_O^t, \mathcal{G}_H^t; \gamma_c)$. We use $\mathcal{R}(\cdot; \gamma)$ to denote a Gaussian rasterizer with camera parameters γ (Fig. 2).

In presence of occlusions, we need to impose certain requirements on the objective function applied to the individual images. In particular, we want to treat areas of occlusion ambiguity differently, such that we do not penalize correct renderings on the individual images. For instance – assuming the object is partially occluding the human – if we simply apply a human mask \mathbf{H}_t^c on the ground truth image \mathbf{I}_t^c and compare it against the rendered human image $\mathbf{I}_{H_t^c}^c$, we would force the occluded human Gaussian parts (invisible in the ground truth image) to disappear. Therefore, we propose a different formulation. The two separately rendered images ($\mathbf{I}_{H_t^c}^c$, $\mathbf{I}_{O_t^c}^c$) are compared against ground-truth human and object images with the pixels for the other entity (i.e. object for human and vice-versa) ignored. For timestep t and camera c , the loss is thus formulated as:

$$\begin{aligned} \mathcal{L}_H^{ct} &= \|\mathbf{I}_t^c \cdot \mathbf{H}_t^c \cdot (1 - \mathbf{O}_t^c) - \mathbf{I}_{H_t^c}^c \cdot (1 - \mathbf{O}_t^c)\|_1 \\ \mathcal{L}_O^{ct} &= \|\mathbf{I}_t^c \cdot \mathbf{O}_t^c \cdot (1 - \mathbf{H}_t^c) - \mathbf{I}_{O_t^c}^c \cdot (1 - \mathbf{H}_t^c)\|_1 \\ \mathcal{L}_A^{ct} &= \|\mathbf{I}_t^c \cdot (\mathbf{O}_t^c + \mathbf{H}_t^c) - \mathbf{I}_{A_t^c}^c\|_1 \end{aligned} \quad (6)$$

and the total \mathcal{L}_1 loss summed over all timesteps and cameras is computed as

$$\mathcal{L}_1 = \sum_{c=1}^{c=N} \sum_{t=1}^{t=T} \mathcal{L}_H^{ct} + \mathcal{L}_O^{ct} + \mathcal{L}_A^{ct}. \quad (7)$$

Our loss is designed to avoid any weight on the pixels for the regions of potential occlusion (Fig. 2). Note that the ignored Gaussians would still be observed and supervised at a different timestep t or camera view c . As we enforce multi-view consistency, our method generates coherent solutions.

Subject:	Human			Object			Full		
Metric:	PSNR↑	SSIM↑	LPIPS↓	PSNR↑	SSIM↑	LPIPS↓	PSNR↑	SSIM↑	LPIPS↓
HUGS [38]	22.13	0.7674	43.71	17.54	0.6878	45.21	21.13	0.7180	42.47
ExAvatar [54]	25.41	0.7743	37.06	16.20	0.5752	37.91	23.18	0.7632	35.58
ToMiE [84]	26.85	0.7700	36.60	20.30	0.6581	35.30	25.49	0.7790	32.33
AnimGau [46]	27.85	0.8900	32.60	23.21	0.7550	37.40	26.49	0.8656	31.43
Ours	28.14	0.9174	28.88	28.63	0.8973	29.77	28.31	0.9242	29.24

Table 1. **Quantitative Results on DNA-Rendering evaluated on held-out images not used during training (all novel human, object and camera poses are not used during training).** We outperform existing baselines that reconstruct animatable 3D humans.

Subject:	Human			Object			Full		
Metric:	PSNR↑	SSIM↑	LPIPS↓	PSNR↑	SSIM↑	LPIPS↓	PSNR↑	SSIM↑	LPIPS↓
HUGS [38]	23.11	0.8274	33.95	19.34	0.6378	47.43	22.12	0.7434	39.47
ExAvatar [54]	25.41	0.8130	34.06	18.35	0.6752	38.99	22.18	0.7820	36.58
ToMiE [84]	23.85	0.7840	34.60	18.51	0.6781	39.40	21.49	0.7260	37.43
AnimGau [46]	26.85	0.8700	26.60	21.50	0.7581	34.40	24.99	0.8160	29.43
Ours	27.64	0.8741	28.46	26.39	0.8732	32.47	26.92	0.8724	29.24

Table 2. **Quantitative Results on the BEHAVE Dataset, evaluated on held-out images not used in training (all human and object poses are unseen in training, but the viewpoint is part of training set as there are only 4 cameras).** We outperform existing baselines that reconstruct animatable 3D humans under occlusion and in presence of objects.

4.6. Learning and Losses

In addition to the \mathcal{L}_1 loss, we also use the perceptual loss [86]. For computing the final perceptual loss, we use the exact masking strategy described in Sec. 4.5.

$$\mathcal{L} = \lambda_{per}\mathcal{L}_{per} + \lambda_{L1}\mathcal{L}_1 + \lambda_{reg}\mathcal{L}_{reg}$$

We further use a \mathcal{L}_{reg} regularization loss to minimize the difference between predicted skinning weights and ground-truth skinning weights of the SMPL template diffused from the SMPL vertices to the canonical human Gaussians.

5. Experiments

We present the first method that reconstructs animatable models of humans and objects under occlusion and as such no straightforward baselines exist for our method. However, in this section we compare our method with recent methods that reconstruct *only* animatable 3D humans from RGB images [38, 46, 54, 84]. All existing methods are designed to work only with humans recorded in isolation with *no occlusion* and are *not designed to handle objects*. While these methods are the closest baselines, note that they are not specifically designed for our task we modify them as detailed in Sec. 5.2. In Sec. 5.3 we demonstrate that unlike *all existing methods* our method allows to animate reconstructed 3D human avatars interacting with novel objects in *novel human poses* and from *novel viewpoints*. We then ablate (Sec. 5.4) the various components of our method.

5.1. Evaluation Dataset

To evaluate our method, we use two datasets of human-object interaction: BEHAVE [8] and DNA-Rendering [11].

BEHAVE dataset [8]. This dataset records eight subjects interacting with a variety of objects. It is captured us-

Subject:	DNA-01			DNA-02			BEH-01		
Metric:	PSNR↑	SSIM↑	LPIPS↓	PSNR↑	SSIM↑	LPIPS↓	PSNR↑	SSIM↑	LPIPS↓
w/o Features	26.11	0.9674	40.95	27.54	0.9678	46.43	25.00	0.9218	59.47
w/o Obj UV	30.41	0.9743	24.06	33.20	0.9752	28.99	26.18	0.9232	35.58
w/o Occ Loss	29.12	0.9727	26.58	32.94	0.9695	36.04	26.63	0.9141	41.76
w/o Obj Track	22.85	0.9600	26.60	23.50	0.9181	31.40	24.49	0.9256	40.43
Full	32.64	0.9774	20.88	33.63	0.9773	25.77	27.64	0.9574	28.46

Table 3. **Ablation Study regarding the various components of our method on the DNA-Rendering and BEHAVE dataset.** As the table indicates, each component in our method adds to the performance and our method cumulatively yields best results. Each line the table corresponds to an experiment detailed in Sec. 5.4

ing four Kinect cameras. We use a subset of each sequence for training and test our method on the remaining held-out frames. Since BEHAVE only uses four cameras, for evaluation we use one of the training cameras.

DNA-Rendering [12]. We also conduct experiments on sequences of the DNA-Rendering dataset. A subset of the DNA-Rendering dataset records people interacting with objects. DNA-Rendering is captured in a studio with sixty RGB cameras. Here again we use a subset of each sequence for training and test our method on the remaining held-out frames. Of the 60 cameras, we use 48 cameras for training and evaluate our method on the rest.

5.2. Baselines

We compare our approach with ExAvatar [54], Animatable-Gaussians [46], HUGS [38] and ToMiE [84] (which as of the submission date does not appear in any conference proceedings). As these methods are primarily designed to reconstruct and animate humans recorded in isolation, they to be modified to deal with objects for a fair comparison. Though ToMiE is designed to reconstruct some objects, it assumes that the object is always attached to the hand, and unlike our method and as such its performance degrades considerably when modelling objects when they detach from the body. Further, *unlike our method, all* baselines, including ToMiE, cannot be used to synthesize humans interacting with new objects. To reconstruct both humans and objects together, we modify the segmentation masks provided in the datasets to include the object along with the humans. All compared methods reconstruct a human using 3dGS, with a canonical space deformed via LBS to posed space and supervised against ground truth pixels. Since we force all these methods to reconstruct the object as well, they are forced to modify the canonical Gaussians even to explain pixels detached from the human body. This results in significant artifacts. The object either disappears or is reconstructed as a blob-like surface, as shown in Fig. 5.

As such, our method significantly outperforms these works when evaluated using standard image quality metrics. This validates our design choice of modeling humans and objects as two separate sets of Gaussians. We report standard metrics computed on the BEHAVE and DNA-Rendering datasets in Tab. 2 and Tab. 1. To evaluate the reconstruction quality of the human and object, we also report



Figure 4. **Top Row:** Qualitative Results of our method on the BEHAVE (right) and DNA-Rendering Datasets (left) using the reconstructed humans and objects in *novel human and object poses*. **Bottom row:** Reconstructed humans animated interacting with *novel objects in novel human poses*.



Figure 5. **Quantitative comparison with existing methods for animatable human reconstruction on BEHAVE (top) and DNA-Rendering (bottom).** Existing methods are unable to reconstruct animatable objects.



Figure 6. UV map ablation. Left: Object learnt using Gaussian maps. Right: Coarse template without Gaussian maps. Representing Gaussian properties as 2D maps captures high frequency details.



Figure 7. Ablation. Left: Gaussians learnt without initializing object poses obtained with tracking. Middle: with tracking. Right: GT



Figure 8. Ablation experiment about occlusion aware loss. From left to right: w/o Occlusion aware loss, with occlusion loss and GT

separate standard image metrics for the human and object. Please note that all metrics are computed for *novel poses* on held out *test images unseen during training*. For the DNA-Rendering dataset we report metrics on novel views while for BEHAVE the training and test camera are same as only 4 cameras are available. In Fig. 4 we show results of our method on BEHAVE and DNA-Rendering.

5.3. Animating Humans with Novel Objects

Since we model the human and object separately, our method allows for animating avatars to interact with novel objects. We do so by animating the reconstructed human Gaussians from one video sequence with object Gaussians, human poses and object poses of another sequence. This allows, *for the first time* in the context of photo-real neural rendering, retargeting of human object interaction from one

sequence to another. If the body shapes of the two avatars differ significantly, the retargeting requires some test-time fine-tuning to ensure plausible contacts. In Fig. 4, we qualitatively demonstrate this ability of our method by animating a reconstructed avatar to interact with novel objects.

5.4. Ablation Studies

In Tab. 3, we evaluate several of our design choices by disabling the respective components. We compare on two sequences from DNA and one from BEHAVE. As the table indicates, each method component improves the results.

Occlusion Loss: In this experiment, we keep all other components of our method unchanged and only switch off the occlusion-aware loss. This forces the occluded regions of the human and object in the rendered image to be part of the background, which degrades reconstruction quality as shown in Fig. 8 and the **w/o Occ Loss** experiment reported in Tab. 3. **Feature Based Reconstruction:** We evaluate the necessity of using a feature based representation to reconstruct coarse object templates by instead optimizing the locations of the 3DGS parameters directly. As the **w/o features** experiment in Tab. 3 shows, without features the template reconstruction does not converge. **Object Tracking:** In this ablation, the object transformation parameters used in Sec. 4.4 are initialized randomly and optimized without being first estimated as described in Sec. 4.2. We find that without proper initialization, these parameters diverge. See **w/o Obj Track** in Tab. 3 and Fig. 7. **Obj UV Map:** In this setting, we do not refine the final object reconstructions using UV maps but generate final renderings using the coarse object template. As shown in Tab. 3 (**w/o Obj UV**) and Fig. 6, the UV map based Gaussian parameter prediction allows for the reconstruction of high-frequency details.

6. Conclusion

We have presented GASPACHO, a method to reconstruct photorealistic human and object interactions from multi-view 2D images, which is capable of human, object and camera pose control. Different from prior art, which only generates photo-real *human actions in empty space* our approach completely decouples the object from the human, enables independent object and human pose control and *for the first time allows for the synthesis of photo-real human animations interacting with novel objects*. We evaluate GASPACHO quantitative and qualitatively on BEHAVE and DNA-Rendering datasets. Our method does make assumptions about the nature of the 3D scenes: *i.e.* we only model one dynamic object and assume that its motion can be explained using only a rigid transform. Future extensions include the reconstruction of humans and objects not only in a lab setting but also from monocular RGB videos collected in the wild. We also hope to extend our work to build autonomous agents that interact not only with small objects but also with large 3D scenes.

References

- [1] Rameen Abdal, Wang Yifan, Zifan Shi, Yinghao Xu, Ryan Po, Zhengfei Kuang, Qifeng Chen, Dit-Yan Yeung, and Gordon Wetzstein. Gaussian shell maps for efficient 3d human generation. In *Proceedings of CVPR*, 2024. 3
- [2] Thiemo Alldieck, Marcus Magnor, Weipeng Xu, Christian Theobalt, and Gerard Pons-Moll. Video based reconstruction of 3d people models. In *IEEE Conference on Computer Vision and Pattern Recognition*. CVPR Spotlight Paper. 3
- [3] Thiemo Alldieck, Marcus Magnor, Bharat Lal Bhatnagar, Christian Theobalt, and Gerard Pons-Moll. Learning to reconstruct people in clothing from a single RGB camera. In *IEEE Conference on Computer Vision and Pattern Recognition (CVPR)*, 2019. 3
- [4] Thiemo Alldieck, Hongyi Xu, and Cristian Sminchisescu. imghum: Implicit generative models of 3d human shape and articulated pose. In *Proceedings of the IEEE/CVF International Conference on Computer Vision*, pages 5461–5470, 2021. 3
- [5] Dragomir Anguelov, Praveen Srinivasan, Daphne Koller, Sebastian Thrun, Jim Rodgers, and James Davis. *SCAPE: Shape Completion and Animation of People*. Association for Computing Machinery, New York, NY, USA, 1 edition, 2023. 2
- [6] Jonathan T Barron, Ben Mildenhall, Dor Verbin, Pratul P Srinivasan, and Peter Hedman. Mip-nerf 360: Unbounded anti-aliased neural radiance fields. In *Proceedings of the IEEE/CVF conference on computer vision and pattern recognition*, pages 5470–5479, 2022. 2
- [7] Jonathan T. Barron, Ben Mildenhall, Dor Verbin, Pratul P. Srinivasan, and Peter Hedman. Zip-nerf: Anti-aliased grid-based neural radiance fields. *ICCV*, 2023. 2
- [8] Bharat Lal Bhatnagar, Xianghui Xie, Ilya A Petrov, Cristian Sminchisescu, Christian Theobalt, and Gerard Pons-Moll. Behave: Dataset and method for tracking human object interactions. In *Proceedings of the IEEE/CVF Conference on Computer Vision and Pattern Recognition*, pages 15935–15946, 2022. 2, 3, 6
- [9] Federica Bogo, Angjoo Kanazawa, Christoph Lassner, Peter Gehler, Javier Romero, and Michael J. Black. Keep it SMPL: Automatic estimation of 3D human pose and shape from a single image. In *Computer Vision – ECCV 2016*. Springer International Publishing, 2016. 3
- [10] Xu Chen, Yufeng Zheng, Michael J Black, Otmar Hilliges, and Andreas Geiger. Snarf: Differentiable forward skinning for animating non-rigid neural implicit shapes. In *International Conference on Computer Vision (ICCV)*, 2021. 3
- [11] Wei Cheng, Ruixiang Chen, Siming Fan, Wanqi Yin, Keyu Chen, Zhongang Cai, Jingbo Wang, Yang Gao, Zhengming Yu, Zhengyu Lin, et al. Dna-rendering: A diverse neural actor repository for high-fidelity human-centric rendering. In *Proceedings of the IEEE/CVF International Conference on Computer Vision*, pages 19982–19993, 2023. 2, 6
- [12] Wei Cheng, Ruixiang Chen, Wanqi Yin, Siming Fan, Keyu Chen, Honglin He, Huiwen Luo, Zhongang Cai, Jingbo Wang, Yang Gao, Zhengming Yu, Zhengyu Lin, Daxuan Ren, Lei Yang, Ziwei Liu, Chen Change Loy, Chen Qian, Wayne Wu, Dahua Lin, Bo Dai, and Kwan-Yee Lin. Dna-rendering: A diverse neural actor repository for high-fidelity human-centric rendering. *arXiv preprint*, arXiv:2307.10173, 2023. 3, 6
- [13] Boyang Deng, John P Lewis, Timothy Jeruzalski, Gerard Pons-Moll, Geoffrey Hinton, Mohammad Norouzi, and Andrea Tagliasacchi. Nasa neural articulated shape approximation. In *Computer Vision–ECCV 2020: 16th European Conference, Glasgow, UK, August 23–28, 2020, Proceedings, Part VII 16*, pages 612–628. Springer, 2020. 3
- [14] Helisa Dharmo, Yinyu Nie, Arthur Moreau, Jifei Song, Richard Shaw, Yiren Zhou, and Eduardo Pérez-Pellitero. Headgas: Real-time animatable head avatars via 3d gaussian splatting. *ECCV*, 2024. 3
- [15] Christian Diller and Angela Dai. Cg-hoi: Contact-guided 3d human-object interaction generation. In *Proc. Computer Vision and Pattern Recognition (CVPR)*, IEEE, 2024. 3
- [16] David F Fouhey, Vincent Delaitre, Abhinav Gupta, Alexei A Efros, Ivan Laptev, and Josef Sivic. People watching: Human actions as a cue for single view geometry. *International journal of computer vision*, 110(3):259–274, 2014. 3
- [17] Antoine Guédon and Vincent Lepetit. Sugar: Surface-aligned gaussian splatting for efficient 3d mesh reconstruction and high-quality mesh rendering. *CVPR*, 2024. 3
- [18] Chen Guo, Tianjian Jiang, Xu Chen, Jie Song, and Otmar Hilliges. Vid2avatar: 3d avatar reconstruction from videos in the wild via self-supervised scene decomposition. In *Proceedings of the IEEE/CVF Conference on Computer Vision and Pattern Recognition (CVPR)*, 2023. 3
- [19] Abhinav Gupta, Scott Satkin, Alexei A Efros, and Martial Hebert. From 3d scene geometry to human workspace. In *CVPR 2011*, pages 1961–1968. IEEE, 2011. 3
- [20] Vladimir Guzov*, Aymen Mir*, Torsten Sattler, and Gerard Pons-Moll. Human positioning system (hps): 3d human pose estimation and self-localization in large scenes from body-mounted sensors. In *IEEE Conference on Computer Vision and Pattern Recognition (CVPR)*. IEEE, 2021. 2, 3
- [21] Marc Habermann, Lingjie Liu, Weipeng Xu, Gerard Pons-Moll, Michael Zollhoefer, and Christian Theobalt. Hdhumans: A hybrid approach for high-fidelity digital humans. 6 (3), 2023. 3
- [22] Mohamed Hassan, Vasileios Choutas, Dimitrios Tzionas, and Michael J. Black. Resolving 3D human pose ambiguities with 3D scene constraints. In *Proceedings International Conference on Computer Vision*, pages 2282–2292. IEEE, 2019. 2, 3
- [23] Mohamed Hassan, Duygu Ceylan, Ruben Villegas, Jun Saito, Jimei Yang, Yi Zhou, and Michael Black. Stochastic Scene-Aware motion prediction. 2021. 2, 3
- [24] Mohamed Hassan, Partha Ghosh, Joachim Tesch, Dimitrios Tzionas, and Michael J. Black. Populating 3D scenes by learning human-scene interaction. In *IEEE/CVF Conf. on Computer Vision and Pattern Recognition (CVPR)*, pages 14708–14718, 2021. 3
- [25] Tong He, Yuanlu Xu, Shunsuke Saito, Stefano Soatto, and Tony Tung. Arch++: Animation-ready clothed human reconstruction revisited. In *Proceedings of the IEEE/CVF interna-*

- tional conference on computer vision, pages 11046–11056, 2021. 3
- [26] Liangxiao Hu, Hongwen Zhang, Yuxiang Zhang, Boyao Zhou, Boning Liu, Shengping Zhang, and Liqiang Nie. Gaussianavatar: Towards realistic human avatar modeling from a single video via animatable 3d gaussians. *arXiv preprint arXiv:2312.02134*, 2023. 2, 4
- [27] Liangxiao Hu, Hongwen Zhang, Yuxiang Zhang, Boyao Zhou, Boning Liu, Shengping Zhang, and Liqiang Nie. Gaussianavatar: Towards realistic human avatar modeling from a single video via animatable 3d gaussians. In *Proceedings of the IEEE/CVF conference on computer vision and pattern recognition*, pages 634–644, 2024. 3
- [28] Binbin Huang, Zehao Yu, Anpei Chen, Andreas Geiger, and Shenghua Gao. 2d gaussian splatting for geometrically accurate radiance fields. In *SIGGRAPH 2024 Conference Papers*. Association for Computing Machinery, 2024. 3
- [29] Zeng Huang, Yuanlu Xu, Christoph Lassner, Hao Li, and Tony Tung. Arch: Animatable reconstruction of clothed humans. In *Proceedings of the IEEE/CVF Conference on Computer Vision and Pattern Recognition*, pages 3093–3102, 2020. 3
- [30] Nan Jiang, Zhiyuan Zhang, Hongjie Li, Xiaoxuan Ma, Zan Wang, Yixin Chen, Tengyu Liu, Yixin Zhu, and Siyuan Huang. Scaling up dynamic human-scene interaction modeling. In *Proceedings of the IEEE/CVF Conference on Computer Vision and Pattern Recognition*, pages 1737–1747, 2024. 3
- [31] Wei Jiang, Kwang Moo Yi, Golnoosh Samei, Oncel Tuzel, and Anurag Ranjan. Neuman: Neural human radiance field from a single video, 2022. 3
- [32] Yuheng Jiang, Suyi Jiang, Guoxing Sun, Zhuo Su, Kaiwen Guo, Minye Wu, Jingyi Yu, and Lan Xu. Neuralhofusion: Neural volumetric rendering under human-object interactions. In *Proceedings of the IEEE/CVF Conference on Computer Vision and Pattern Recognition*, pages 6155–6165, 2022. 2
- [33] Yuheng Jiang, Zhehao Shen, Yu Hong, Chengcheng Guo, Yize Wu, Yingliang Zhang, Jingyi Yu, and Lan Xu. Robust dual gaussian splatting for immersive human-centric volumetric videos. *arXiv preprint arXiv:2409.08353*, 2024. 3
- [34] Angjoo Kanazawa, Michael J. Black, David W. Jacobs, and Jitendra Malik. End-to-end recovery of human shape and pose. In *Computer Vision and Pattern Recognition (CVPR)*, 2018. 3
- [35] Tero Karras, Samuli Laine, and Timo Aila. A style-based generator architecture for generative adversarial networks. In *Proceedings of the IEEE/CVF conference on computer vision and pattern recognition*, pages 4401–4410, 2019. 4
- [36] Nikhil Keetha, Jay Karhade, Krishna Murthy Jatavallabhula, Gengshan Yang, Sebastian Scherer, Deva Ramanan, and Jonathon Luiten. Splatam: Splat, track & map 3d gaussians for dense rgb-d slam. In *Proceedings of the IEEE/CVF Conference on Computer Vision and Pattern Recognition*, 2024. 3
- [37] Bernhard Kerbl, Georgios Kopanas, Thomas Leimkühler, and George Drettakis. 3d gaussian splatting for real-time radiance field rendering. *ACM Transactions on Graphics*, 42(4), 2023. 1, 2, 3
- [38] Muhammed Kocabas, Jen-Hao Rick Chang, James Gabriel, Oncel Tuzel, and Anurag Ranjan. Hugs: Human gaussian splats. *arXiv preprint arXiv:2311.17910*, 2023. 2, 3, 6, 7
- [39] Christoph Lassner and Michael Zollhöfer. Pulsar: Efficient sphere-based neural rendering. In *IEEE/CVF Conference on Computer Vision and Pattern Recognition (CVPR)*, 2021. 2
- [40] Junoh Lee, Changyeon Won, Hyunjun Jung, Inhwan Bae, and Hae-Gon Jeon. Fully explicit dynamic gaussian splatting. In *Proceedings of the Neural Information Processing Systems*, 2024. 3
- [41] Jiahui Lei, Yufu Wang, Georgios Pavlakos, Lingjie Liu, and Kostas Daniilidis. Gart: Gaussian articulated template models. *arXiv preprint arXiv:2311.16099*, 2023. 3
- [42] J. P. Lewis, Matt Corder, and Nickson Fong. *Pose Space Deformation: A Unified Approach to Shape Interpolation and Skeleton-Driven Deformation*. Association for Computing Machinery, New York, NY, USA, 1 edition, 2023. 2
- [43] Ruilong Li, Julian Tanke, Minh Vo, Michael Zollhofer, Jürgen Gall, Angjoo Kanazawa, and Christoph Lassner. Tava: Template-free animatable volumetric actors. In *European Conference on Computer Vision (ECCV)*, 2022. 3
- [44] Zhan Li, Zhang Chen, Zhong Li, and Yi Xu. Spacetime gaussian feature splatting for real-time dynamic view synthesis. *arXiv preprint arXiv:2312.16812*, 2023. 3
- [45] Zhe Li, Yipengjing Sun, Zerong Zheng, Lizhen Wang, Shengping Zhang, and Yebin Liu. Animatable and relightable gaussians for high-fidelity human avatar modeling. *arXiv preprint arXiv:2311.16096v4*, 2024. 3
- [46] Zhe Li, Zerong Zheng, Lizhen Wang, and Yebin Liu. Animatable gaussians: Learning pose-dependent gaussian maps for high-fidelity human avatar modeling. In *Proceedings of the IEEE/CVF Conference on Computer Vision and Pattern Recognition (CVPR)*, 2024. 2, 3, 4, 6, 7
- [47] Jia-Wei Liu, Yan-Pei Cao, Tianyuan Yang, Zhongcong Xu, Jussi Keppo, Ying Shan, Xiaohu Qie, and Mike Zheng Shou. Hosnerf: Dynamic human-object-scene neural radiance fields from a single video. In *Proceedings of the IEEE/CVF International Conference on Computer Vision*, pages 18483–18494, 2023. 2
- [48] Lingjie Liu, Marc Habermann, Viktor Rudnev, Kripasindhu Sarkar, Jiatao Gu, and Christian Theobalt. Neural actor: Neural free-view synthesis of human actors with pose control. *ACM Trans. Graph.(ACM SIGGRAPH Asia)*, 2021. 3
- [49] Matthew Loper, Naureen Mahmood, Javier Romero, Gerard Pons-Moll, and Michael J. Black. SMPL: A skinned multi-person linear model. *ACM Trans. Graphics (Proc. SIGGRAPH Asia)*, 34(6):248:1–248:16, 2015. 2, 3
- [50] Jonathon Luiten, Georgios Kopanas, Bastian Leibe, and Deva Ramanan. Dynamic 3d gaussians: Tracking by persistent dynamic view synthesis. In *3DV*, 2024. 3
- [51] Lars Mescheder, Michael Oechsle, Michael Niemeyer, Sebastian Nowozin, and Andreas Geiger. Occupancy networks: Learning 3d reconstruction in function space. In *Proceedings of the IEEE/CVF conference on computer vision and pattern recognition*, pages 4460–4470, 2019. 3

- [52] Marko Mihajlovic, Sergey Prokudin, Siyu Tang, Robert Maier, Federica Bogo, Tony Tung, and Edmond Boyer. SplatFields: Neural gaussian splats for sparse 3d and 4d reconstruction. In *European Conference on Computer Vision (ECCV)*. Springer, 2024. 3
- [53] Ben Mildenhall, Pratul P. Srinivasan, Matthew Tancik, Jonathan T. Barron, Ravi Ramamoorthi, and Ren Ng. Nerf: Representing scenes as neural radiance fields for view synthesis. In *ECCV*, 2020. 2
- [54] Gyeongsik Moon, Takaaki Shiratori, and Shunsuke Saito. Expressive whole-body 3D gaussian avatar. In *ECCV*, 2024. 2, 3, 6, 7
- [55] Arthur Moreau, Jifei Song, Helisa Dharmo, Richard Shaw, Yiren Zhou, and Eduardo Pérez-Pellitero. Human gaussian splatting: Real-time rendering of animatable avatars. In *Proceedings of the IEEE/CVF Conference on Computer Vision and Pattern Recognition*, pages 788–798, 2024. 2, 3
- [56] Thomas Müller, Alex Evans, Christoph Schied, and Alexander Keller. Instant neural graphics primitives with a multiresolution hash encoding. *ACM Trans. Graph.*, 41(4):102:1–102:15, 2022. 2
- [57] Haokai Pang, Heming Zhu, Adam Kortylewski, Christian Theobalt, and Marc Habermann. Ash: Animatable gaussian splats for efficient and photoreal human rendering. *arXiv preprint arXiv:2312.05941*, 2023. 2
- [58] Haokai Pang, Heming Zhu, Adam Kortylewski, Christian Theobalt, and Marc Habermann. Ash: Animatable gaussian splats for efficient and photoreal human rendering. In *Proceedings of the IEEE/CVF Conference on Computer Vision and Pattern Recognition*, pages 1165–1175, 2024. 3, 4
- [59] Jeong Joon Park, Peter Florence, Julian Straub, Richard Newcombe, and Steven Lovegrove. DeepSDF: Learning continuous signed distance functions for shape representation. In *Proceedings of the IEEE/CVF conference on computer vision and pattern recognition*, pages 165–174, 2019. 3
- [60] Georgios Pavlakos, Vasileios Choutas, Nima Ghorbani, Timo Bolkart, Ahmed A. A. Osman, Dimitrios Tzionas, and Michael J. Black. Expressive body capture: 3D hands, face, and body from a single image. In *Proceedings IEEE Conf. on Computer Vision and Pattern Recognition (CVPR)*, pages 10975–10985, 2019. 3
- [61] Sida Peng, Junting Dong, Qianqian Wang, Shangzhan Zhang, Qing Shuai, Xiaowei Zhou, and Hujun Bao. Animatable neural radiance fields for modeling dynamic human bodies. In *ICCV*, 2021. 3
- [62] Zhiyin Qian, Shaofei Wang, Marko Mihajlovic, Andreas Geiger, and Siyu Tang. 3dgs-avatar: Animatable avatars via deformable 3d gaussian splatting. *arXiv preprint arXiv:2312.09228*, 2023. 2, 3
- [63] Zhiyin Qian, Shaofei Wang, Marko Mihajlovic, Andreas Geiger, and Siyu Tang. 3dgs-avatar: Animatable avatars via deformable 3d gaussian splatting. 2024. 3
- [64] Shunsuke Saito, Tomas Simon, Jason Saragih, and Hanbyul Joo. Pifuhd: Multi-level pixel-aligned implicit function for high-resolution 3d human digitization. In *CVPR*, 2020. 3
- [65] Manolis Savva, Angel X. Chang, Pat Hanrahan, Matthew Fisher, and Matthias Nießner. PiGraphs: Learning Interaction Snapshots from Observations. *ACM Transactions on Graphics (TOG)*, 35(4), 2016. 3
- [66] Richard Shaw, Jifei Song, Arthur Moreau, Michal Nazarczuk, Sibi Catley-Chandar, Helisa Dharmo, and Eduardo Perez-Pellitero. Swags: Sampling windows adaptively for dynamic 3d gaussian splatting. *arXiv preprint arXiv:2312.13308*, 2023. 3
- [67] Sebastian Starke, He Zhang, Taku Komura, and Jun Saito. Neural state machine for character-scene interactions. *ACM Trans. Graph.*, 38(6), 2019. 3
- [68] Guoxing Sun, Xin Chen, Yizhang Chen, Anqi Pang, Pei Lin, Yuheng Jiang, Lan Xu, Jingyi Yu, and Jingya Wang. Neural free-viewpoint performance rendering under complex human-object interactions. In *Proceedings of the 29th ACM International Conference on Multimedia*, pages 4651–4660, 2021. 2
- [69] Omid Taheri, Nima Ghorbani, Michael J. Black, and Dimitrios Tzionas. GRAB: A dataset of whole-body human grasping of objects. In *European Conference on Computer Vision (ECCV)*, 2020. 3
- [70] Matthew Tancik, Ethan Weber, Evonne Ng, Ruilong Li, Brent Yi, Justin Kerr, Terrance Wang, Alexander Kristoffersen, Jake Austin, Kamyar Salahi, Abhik Ahuja, David McAllister, and Angjoo Kanazawa. Nerfstudio: A modular framework for neural radiance field development. In *ACM SIGGRAPH 2023 Conference Proceedings*, 2023. 2
- [71] Xiaolong Wang, Rohit Girdhar, and Abhinav Gupta. Binge watching: Scaling affordance learning from sitcoms. In *Proceedings of the IEEE Conference on Computer Vision and Pattern Recognition*, pages 2596–2605, 2017. 3
- [72] Jing Wen, Xiaoming Zhao, Zhongzheng Ren, Alex Schwing, and Shenlong Wang. GoMAAvatar: Efficient Animatable Human Modeling from Monocular Video Using Gaussians-on-Mesh. In *CVPR*, 2024. 2
- [73] Chung-Yi Weng, Brian Curless, Pratul P. Srinivasan, Jonathan T. Barron, and Ira Kemelmacher-Shlizerman. HumanNeRF: Free-viewpoint rendering of moving people from monocular video. In *Proceedings of the IEEE/CVF Conference on Computer Vision and Pattern Recognition (CVPR)*, pages 16210–16220, 2022. 3
- [74] Lee Alan Westover. *Splatting: a parallel, feed-forward volume rendering algorithm*. PhD thesis, USA, 1992. 2
- [75] Guanjun Wu, Taoran Yi, Jiemin Fang, Lingxi Xie, Xiaopeng Zhang, Wei Wei, Wenyu Liu, Qi Tian, and Xinggang Wang. 4d gaussian splatting for real-time dynamic scene rendering. In *Proceedings of the IEEE/CVF Conference on Computer Vision and Pattern Recognition (CVPR)*, pages 20310–20320, 2024. 3
- [76] Xianghui Xie, Bharat Lal Bhatnagar, and Gerard Pons-Moll. Chore: Contact, human and object reconstruction from a single rgb image. In *European Conference on Computer Vision (ECCV)*. Springer, 2022. 3
- [77] Xianghui Xie, Bharat Lal Bhatnagar, and Gerard Pons-Moll. Visibility aware human-object interaction tracking from single rgb camera. In *IEEE Conference on Computer Vision and Pattern Recognition (CVPR)*, 2023.

- [78] Xianghui Xie, Bharat Lal Bhatnagar, Jan Eric Lenssen, and Gerard Pons-Moll. Template free reconstruction of human-object interaction with procedural interaction generation. In *Proceedings of the IEEE/CVF Conference on Computer Vision and Pattern Recognition*, pages 10003–10015, 2024. 3
- [79] Yiheng Xie, Towaki Takikawa, Shunsuke Saito, Or Litany, Shiqin Yan, Numair Khan, Federico Tombari, James Tompkin, Vincent Sitzmann, and Srinath Sridhar. Neural fields in visual computing and beyond. *Computer Graphics Forum*, 2022. 2
- [80] Hongyi Xu, Eduard Gabriel Bazavan, Andrei Zanfir, William T Freeman, Rahul Sukthankar, and Cristian Sminchisescu. Ghum & ghuml: Generative 3d human shape and articulated pose models. In *Proceedings of the IEEE/CVF Conference on Computer Vision and Pattern Recognition*, pages 6184–6193, 2020. 2
- [81] Hongyi Xu, Thiemo Alldieck, and Cristian Sminchisescu. H-nerf: Neural radiance fields for rendering and temporal reconstruction of humans in motion. *Advances in Neural Information Processing Systems*, 34:14955–14966, 2021. 3
- [82] Yuelang Xu, Benwang Chen, Zhe Li, Hongwen Zhang, Lizhen Wang, Zerong Zheng, and Yebin Liu. Gaussian head avatar: Ultra high-fidelity head avatar via dynamic gaussians. In *Proceedings of the IEEE/CVF Conference on Computer Vision and Pattern Recognition*, pages 1931–1941, 2024. 3
- [83] Lixin Xue, Chen Guo, Chengwei Zheng, Fangjinhua Wang, Tianjian Jiang, Hsuan-I Ho, Manuel Kaufmann, Jie Song, and Hilliges Otmar. HSR: holistic 3d human-scene reconstruction from monocular videos. In *European Conference on Computer Vision (ECCV)*, 2024. 2, 3
- [84] Yifan Zhan, Qingtian Zhu, Muyao Niu, Mingze Ma, Jiancheng Zhao, Zhihang Zhong, Xiao Sun, Yu Qiao, and Yinqiang Zheng. Tomie: Towards modular growth in enhanced smpl skeleton for 3d human with animatable garments, 2024. 2, 3, 6, 7
- [85] Jason Y. Zhang, Sam PePose, Hanbyul Joo, Deva Ramanan, Jitendra Malik, and Angjoo Kanazawa. Perceiving 3d human-object spatial arrangements from a single image in the wild. In *European Conference on Computer Vision (ECCV)*, 2020. 3
- [86] Richard Zhang, Phillip Isola, Alexei A Efros, Eli Shechtman, and Oliver Wang. The unreasonable effectiveness of deep features as a perceptual metric. In *Proceedings of the IEEE conference on computer vision and pattern recognition*, pages 586–595, 2018. 6
- [87] Xiaohan Zhang, Bharat Lal Bhatnagar, Sebastian Starke, Vladimir Guzov, and Gerard Pons-Moll. Couch: Towards controllable human-chair interactions. *European Conference on Computer Vision (ECCV)*, 2022. 2, 3
- [88] Shunyuan Zheng, Boyao Zhou, Ruizhi Shao, Boning Liu, Shengping Zhang, Liqiang Nie, and Yebin Liu. Gps-gaussian: Generalizable pixel-wise 3d gaussian splatting for real-time human novel view synthesis. In *Proceedings of the IEEE/CVF Conference on Computer Vision and Pattern Recognition (CVPR)*, 2024. 3
- [89] Heming Zhu, Fangneng Zhan, Christian Theobalt, and Marc Habermann. Trihuman: A real-time and controllable tri-plane representation for detailed human geometry and appearance synthesis. *ACM Trans. Graph.*, 2024. 2, 3
- [90] Wojciech Zielonka, Timur Bagautdinov, Shunsuke Saito, Michael Zollhöfer, Justus Thies, and Javier Romero. Drivable 3d gaussian avatars. *arXiv preprint arXiv:2311.08581*, 2023. 3
- [91] Matthias Zwicker, Hanspeter Pfister, Jeroen van Baar, and Markus Gross. Surface splatting. In *Proceedings of the 28th Annual Conference on Computer Graphics and Interactive Techniques*, page 371–378, New York, NY, USA, 2001. Association for Computing Machinery. 3